
This is an electronic reprint of the original article.
This reprint may differ from the original in pagination and typographic detail.

Yazdani, Maryam Roza; Lagerström, Anna; Vuorinen, Ville

Simultaneous effect of biochar-additive and lightweight heat exchanger on phase change material for low-grade thermal energy storage

Published in:
Journal of Energy Storage

DOI:
[10.1016/j.est.2022.105478](https://doi.org/10.1016/j.est.2022.105478)

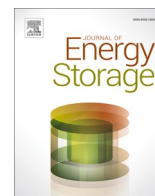
Published: 15/11/2022

Document Version
Publisher's PDF, also known as Version of record

Published under the following license:
CC BY

Please cite the original version:
Yazdani, M. R., Lagerström, A., & Vuorinen, V. (2022). Simultaneous effect of biochar-additive and lightweight heat exchanger on phase change material for low-grade thermal energy storage. *Journal of Energy Storage*, 55, Article 105478. <https://doi.org/10.1016/j.est.2022.105478>

This material is protected by copyright and other intellectual property rights, and duplication or sale of all or part of any of the repository collections is not permitted, except that material may be duplicated by you for your research use or educational purposes in electronic or print form. You must obtain permission for any other use. Electronic or print copies may not be offered, whether for sale or otherwise to anyone who is not an authorised user.



Research papers

Simultaneous effect of biochar-additive and lightweight heat exchanger on phase change material for low-grade thermal energy storage

Maryam Roza Yazdani^{*}, Anna Lagerström, Ville Vuorinen

Department of Mechanical Engineering, Aalto University, FI-00076 Aalto, Finland



ARTICLE INFO

Keywords:

Thermal energy storage
Phase change material (PCM)
Heat transfer
Heat exchanger
Biochar additive
Smart heating

ABSTRACT

In this paper, we report the experimental performance of a low to medium temperature (20–50 °C) latent heat storage (LHS) system. The power and temperature ranges of the LHS have relevance to various applications such as heat sink and storage for high-power electronics devices and low-temperature district heating (LTDH). This new LHS includes a lightweight heat exchanger (LHE) with a complex heat transfer area for organic phase change materials (PCMs). The model PCMs provide a medium-low phase transition temperature range, namely decanoic acid (DA) and a commercial PCM. To facilitate the storage performance of the system, biochar (BC) additive is further investigated to simultaneously enhance the thermal properties of the PCM within the LHE. The PCMs are characterized using common material characterization methods such as differential scanning calorimetry, X-ray diffraction, and scanning electron microscopy. The system investigation focuses on the effect of the heat exchanger, the PCM type and the additive concentration on the duration and power of charging-discharging cycle as well as the storage capacity. Two weight percentages (1 % and 2 %) of BC were studied, while the addition of 1 % BC to DA resulted in the most effective storage performance in both the system (444 kJ storage capacity) and characterization (170.5 kJ/kg melting enthalpy) experiments. The lightweight structure of the grid enabled loading of a large PCM amount (1.84 kg) as well as swift charging (430 W during 25 min). The system indicated a cooperative enhancement with BC additive as the charging power increased by 32 % (570 W) and charging time decreased by 33 % (17 min). A conceptual modular design of the investigated system is proposed to heat up the floor or the bench of a smart city bus stop. The modular unit of ten integrated LHEs filled with BC enhanced DA is estimated to provide 1.2 kWh storage capacity sufficient for heating the bus floor for 6 h or the bus bench for 15 h. This is a potential solution for reclaiming the excess heat from LTDH substations, while buffering their undesired temperature variations.

1. Introduction

The time and location discrepancies between the energy supply and energy demand challenge the development of sustainable energy systems utilizing renewable energy resources. Viable energy storage solutions are thus essential for the implementation of intermittent renewable energy [1,2]. Thermal energy storage (TES) is a key method to incorporate renewable in energy systems. TES improves the energy efficiency and reduces the energy consumption by reclaiming the waste heat.

Sensible heat storage (SHS) is the conventional method of storing sensible heat, typically requiring large volumes and operation temperature ranges. The implementation of SHS is limited to mainly centralized storage tanks that can be inconvenient or impractical for urban settings due to the expensive and laborious reconstruction of already existing

infrastructure. Contrarily, latent heat storage (LHS) offers an attractive way to store energy that can overcome the challenges related to SHS. The LHS stores and releases energy as latent heat of phase change materials (PCMs) during their melting and crystallization reactions [3,4]. PCMs provide a high energy storage density while operating in narrower temperature ranges. For example, they can store around 2.5–6 times more energy compared to that of sensible water storage over a 20 °C temperature range [5,6]. Therefore, PCMs have attracted interest in various industrial and residential applications for storing energy, reducing waste heat, or peak-shaving [7].

The LHS units could be incorporated within domestic heating systems utilizing water radiators as well as centralized ventilation systems. Morales-Ruiz et al. [8] employed LHS for waste heat recovery from the drain water of a domestic washing machine containing a significant

^{*} Corresponding author.

E-mail address: roza.yazdani@aalto.fi (M.R. Yazdani).

<https://doi.org/10.1016/j.est.2022.105478>

Received 24 December 2021; Received in revised form 15 July 2022; Accepted 9 August 2022

Available online 29 August 2022

2352-152X/© 2022 The Author(s). Published by Elsevier Ltd. This is an open access article under the CC BY license (<http://creativecommons.org/licenses/by/4.0/>).

amount of waste heat. The LHS was also studied in low-temperature district heating (LDH) networks to increase the system efficiency via buffering the temperature variations between the supply and the demand [9]. A LHS system using a salt hydrate with a melting temperature around 20 °C was explored for cooling a data center [10]. Solar and electric systems are among other existing applications of LHS [11–13].

The integration of LHS into the heating or cooling systems usually requires a PCM reactor embedding a heat exchanger (HE) and a heat transfer fluid (HTF) such as water or air [5]. The bottleneck of this technology, however, is the low thermal conductivity (TC) of most PCMs that significantly limits the storage efficiency, the charging and discharging rates, and the temperature distribution within the storage. Fin-based extended metal surfaces for the HEs [14,15] and conductive additives for the PCMs [6,14,16] have been explored to enhance the heat transfer within LHS systems. The differences between finned HEs and additives for this purpose is that the former improves the heat exchange area between PCM and HTF, while the latter enhances the thermophysical properties of the PCMs e.g., thermal conductivity, specific heat capacity and latent heat. The shell-and-tube HE design with the HTF circulating inside the tube and paraffin-based PCMs filling the shell part with various fin structures are the most studied configuration for medium-temperature TES applications [14,17,18]. The tube-and-shell design, however, suffer from several practical issues such as drastic temperature stratification of the storage and insufficient heat transfer rate leading to prolonged charging time and reduced efficiency of system [19,20]. The addition of additives, on the other hand, can increase TC and crystallization rate, but it may obstruct and reduce the effect of natural convection and melting time in the system. This can however be solved through the adjustment of its added amount into the system [21]. As such, combining these two approaches, as was done in this work, is appealing to simultaneously improve the thermal properties of the PCM as well as the heat exchange area of the HE.

The increasing demand for incorporating renewable and reclaiming waste calls for developing more efficient and advanced energy storage designs that can be tailored according to the target application requirements such as the charging temperature, charging time, and system efficiency. We have designed a new type of heat exchanger with large extended metal surfaces in the form of grid structure which solves the practical issues related to tube-and-shell design. The highly complex grid structure was enabled with the emerging production method of 3D printing that has remained fairly unexplored in energy utilization field. Contrary to tube-and-shell design, the grid structure provides a more uniform temperature variation within the storage and increases the charging rate more effectively. Previously, we studied three grid geometries that provided high charging and discharging rates and storage power with a medium-temperature paraffin PCM [22]. However, there is still a knowledge gap for such experimental system research using low-melting point PCMs for low-temperature LHS suitable in low-grade waste heat recovery. Furthermore, there is a high derive for bio-based materials with renewable origin to replace fossil-fuel based products, which justifies further investigation of bio-based PCMs such as fatty acids as an alternative to fossil-fuel based paraffin.

In this study, we aim at developing the grid HE as lightweight as possible by reducing the thickness of the extended surfaces, making the design more sustainable, cost-effective and easier-to-handle due to less usage of critical metal material. A lightweight feature enabled a less usage of metal alloy in the grid structure (915 g and 253 ml) and reduced the used metal cost by 33 %, compared to those of the heavier tapering design (1364 g and 472 ml) in our previous work [22]. This opened more space to insert PCM (46 % increase) and consequently increased the storage capacity by 19 %. We further investigate the cooperative effect of low-cast and locally-available biocarbon additives in the system. The simultaneous effect of additives and heat exchangers on PCMs is scarcely studied. Carbon additives have attracted great interest for enhancing the thermal performance of PCMs due to their thermal capacity, low density, and stable chemical nature [23]. Studies have indicated that various

concentrations and addition techniques of additives to different PCMs can cause a wide range of outcomes on their thermal properties. For example, carbon particles can increase the heat transfer within PCM storage, while often reducing their latent heat capacity when used in excessive amounts [23]. Therefore, the concentration of the additive needs further consideration. One promising material in this category is biochar (BC) that is carbonized biomass such as wood, algae, and sludge. Biochar has recently attracted a great research interest for various applications thanks to its low-cast, eco-friendliness, local-availability, and great thermal properties [24–26]. To the best of our knowledge, BC has not been yet investigated as additives in system level energy storage experiments, particularly, not in combination with grid type HE.

Herein, we investigated the new lightweight 3D-printed grid HE embedding two different organic PCMs, namely decanoic acid and PlusICE A28 commercial PCM, with a low-melting temperature (T_m) around 30 °C. The selection of the PCMs was based on providing a melting temperature that is relevant for the recovery of low-grade heat and low temperature district heating as the target application (20–50 °C). Fatty acids provide promising material properties such as low-cost, high latent heat, and plant-based renewable origin [27,28]. Nevertheless, there is an evident knowledge gap in their potential use in system-level LHS studies. We further validated the performance of the storage with a commercial PCM to ensure that the concept is applicable for different available PCMs. The low thermal conductivity of such organic PCMs (0.150–0.413 W/mK [27,28]) however justifies the use of effective heat transfer enhancement methods for their implementation in system-level LHS. Thus, we exploited the simultaneous effect of BC additives and grid HE to enhance the heat exchange within the LHS incorporating fatty acids. To the best of our knowledge, such a configuration has not been reported elsewhere. Two low mass concentrations, 1 % and 2 %, of BC were tested. To understand the nature of interactions between the PCM and the additive, the mixtures of the PCM with BC were characterized with common material characterization methods such as differential scanning calorimetry (DSC), X-ray diffraction (XRD) and optical and scanning electron microscopy. The addition of BC in a minimal weight percentage (1 %) improved the thermal properties of the PCM e.g. latent heat, specific heat and thermal conductivity that resulted in an increase in storage performance of the system. A conceptual modular design of the investigated system was proposed for the heat management of a conceptual smart city bus stop.

2. Research methodology

2.1. Materials and characterizations

Decanoic acid (DA) was supplied by VWR (ACROS Organics 99 % purity). PlusICE A28 (PCA28) commercial PCM was provided by PCM Products Ltd. Biochar (BC) was supplied by Carbons Finland Oy. It was produced through carbonization of spruce wood at 600 °C in a nitrogen gas environment. Prior to the addition of the PCM, the BC was first ground and sieved to a fine powder of less than 50 µm size and a bulk density of 0.23 kg/l. A 1 % or 2 % (wt%) concentration of the BC powder was then mixed with the PCM melt for 2 h to obtain a uniform mixture.

Differential scanning calorimetry (DSC) was performed with Netzsch DSC204F1 Phoenix instrument to measure the phase change temperature and enthalpy of the PCMs. Three separate replicates were measured with a sample size between 10 and 15 mg. The DSC program included four consecutive heating and cooling cycles within 0–50 °C temperature range under 5 K/min scan rate. The specific heat measurements were based on the Sapphire correction of the DSC program. The thermal conductivity was measured with a C-Therm thermal conductivity analyzer [29] using solid PCM disk samples with a 35 cm diameter and 1 cm height. The thermal conductivity of BC was measured in a powder form. Supplementary Information includes an illustration of conductivity measurement set-up and samples. X-ray diffraction (XRD) was conducted on a Rigaku SmartLab X-ray diffractometer. Polarized optical

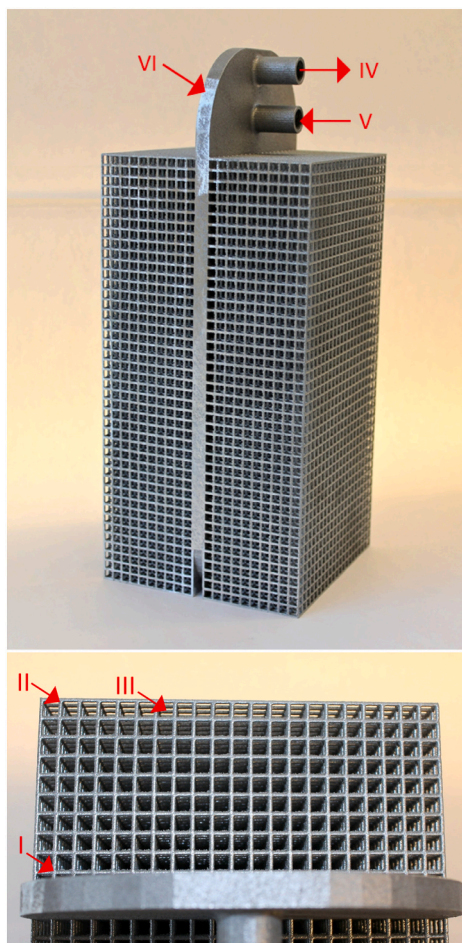


Fig. 1. The lightweight heat exchanger (LHE) and the closeup view of the grid geometry: I grid thickness at the base (1 mm), II grid thickness at the tip (0.75 mm), III grid spacing (4 mm to 4.25 mm), VI base plate where HTF circulates, V HTF inlet, and IV HTF outlet.

microscopy (POM) was conducted on a Leica DM4500 optical microscope. Scanning electron microscopy (SEM) was carried out on a Zeiss Sigma VP microscope (Germany) at 2 kV accelerated voltage. The samples were coated with a thin layer of gold palladium alloy (4 nm) using a sputter coater (LECIA EM ACE600) before the SEM observation.

2.2. Lightweight design of the heat exchanger

A lightweight heat exchanger (LHE) was 3D-printed with aluminum-silicon (AlSi10Mg) alloy using a powder bed fusion technology by the FIT Additive Manufacturing Group. The skeleton design of the HE was adopted from a tapering configuration reported in our previous work [22]. It included two parts: a base plate for the HTF circulation (see Fig. A in the Supplementary Information) and an extruded grid structure from the base plate throughout the storage tank to transfer the heat from the HTF within the inserted PCM. Herein, we aimed at minimizing the volume of the HE via reducing the thickness of the grid and consequently to create extra free space for loading a larger PCM volume into the storage tank. This allowed less metal alloy for the production of the HE, which made the product cheaper and more sustainable. As seen in Fig. 1, the grid included orthogonal tapering rows starting from 1 mm thickness (I) at the base plate (VI) and ending with 0.75 mm thickness (II) at the tip. The grid spacing (III) varied from 4.0 mm at the base to 4.25 mm at the tip. The parallel rows to the plate part were set at 0.75 mm thickness. The volume and mass of LHE were 253 ml and 915 g, respectively, providing considerable reductions in volume (46 %) and mass (33 %)

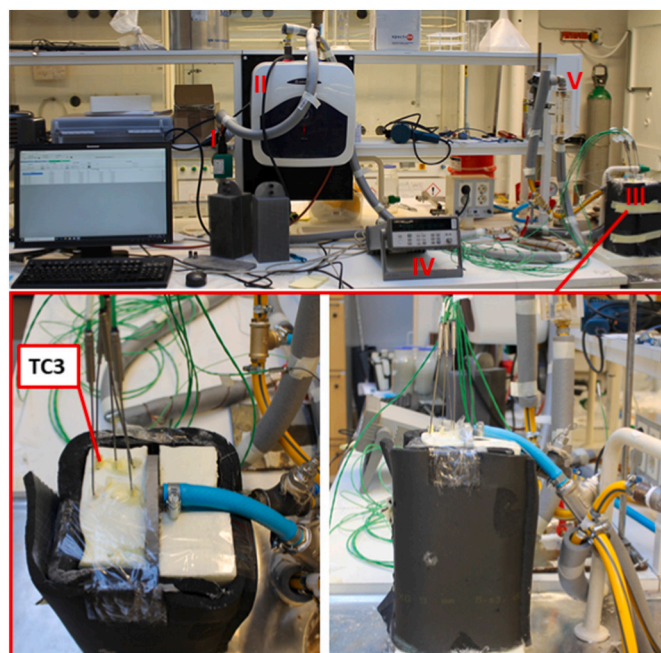


Fig. 2. The lab-scale latent heat storage system and insulated PCM storage tank embedding HE and thermocouples: I pump, II the heat source boiler, III storage tank IV data collector and V flow-meter. See Fig. B in the Supplementary Information for enlarged images of each component and PID of the system.

compared to those of the tapering configuration (472 ml and 1364 g) in our previous work [22]. Such a lightweight design could benefit larger-scale applications due to the cost reduction by the decreased metal content of the HE, while increasing the PCM amount and storage capacity of the system.

2.3. Lab-scale latent heat thermal energy storage system

The LHS experimental setup is shown in Fig. 2, which consisted of charging and discharging loops equipped with (I) a water pump, (II) heating source (Ariston BLU EVO R 10/3 EU boiler), (III) an insulated PCM tank, (IV) data acquisition system and (V) flow-meter. The piping and instrumentation diagram (PID) and images of system components are provided in Fig. B in the Supplementary Information. The HE was immersed in the storage tank filled with the PCM. A voltage regulator was added to the system to stabilize the operation of the pump and an expansion tank (5 bar, 8 l) was used to release water pressure created during the storage process. Water was used as heat transfer fluid (HTF), circulating within the system at a flow rate of 2.5 kg/min. The temperature of PCM was measured by five K-type thermocouples, calibrated with 2.2 °C accuracy. The thermocouples were placed in the middle vertical height of the tank and at the following horizontal locations: two at 1 cm distance to the base plate, one at the middle (2.5 cm) distance, and two at 4.5 cm distance closer to the tank edge. The installation of thermocouples in the insulated tank is displayed in Fig. 2. Two extra thermocouples measured the temperature of inflow and outflow HTF at the inlet and outlet of the HE.

A full experiment cycle consisted of a charging and discharging process. To ensure the complete melting of PCM in the storage tank, the charging was continued until all thermocouples indicated at least 50 °C. The charging loop was then switched to the discharging loop, providing cold water from the tap to the inflow of the HE. Discharging process was continued until all thermocouples within the PCM had reached at least to room temperature (22 °C). The experiments for each PCM were repeated at least three times to obtain consistent and comparable data.

The total amount of stored energy in the PCM storage during the

Table 1

Thermophysical properties of pristine and BC-enhanced PCMs. The latent heat was measured as the area below the corresponding DSC peak. The melting temperature was assigned to the peak value, where the PCM has completely transformed to its liquid phase. The specific heat was measured as the mean value within 0–15 °C temperature range on heating (before melting) for solid and within 40–50 °C (after melting) for liquid.

	PCA28	DA	1 % BC	2 % BC
$c_{p,s}$ (kJ/kgK)	1.42	1.89	2.14	1.86
$c_{p,l}$ (kJ/kgK)	1.73	2.13	2.30	2.05
T_m (°C)	32.9	36	12.9	15.3
ΔH_c (kJ/kg)	242	164.2	175.5	157.8
ΔH_m (kJ/kg)	247.6	161.1	170.5	155.6
Density (kg/l)	0.70	0.81	0.80	0.81
TC (W/mK)	0.99	0.52	0.60	0.62

charging process includes both sensible heat, Q_s , and latent heat, Q_l . Sensible heat depends on the specific heat of the PCM, while latent heat is related to the enthalpy of phase change. The total amount of stored energy (Q_t) can be calculated with Eq. (1):

$$Q_t = Q_s + Q_l = m_{pcm}(C_{p,s}\Delta T_s + \Delta H_m + C_{p,l}\Delta T_l) \quad (1)$$

where m_{pcm} is the mass of the PCM. $C_{p,s}$ and $C_{p,l}$ are the specific heat values and ΔT_s and ΔT_l are the temperature ranges for the PCM in solid and liquid states, respectively. ΔH_m is the latent heat of melting. The storage power can be determined with Eq. (2):

$$P = m_{hif}C_p(T_{of} - T_{if}) \quad (2)$$

where m_{hif} is the mass flow of HTF. C_p is the specific heat of water (4187 kJ/kgK). T_{of} and T_{if} are the water temperature measured at the outflow

and the inflow of the HE, respectively.

2.4. Application conceptualization

To put the experimental data in a context, a case study was made to feature a conceptual LHS design for a smart bus stop, including the calculation of the demand, cost and duration of heating supply based on the storage size. The study was performed for the LHE filled with 1 % BC-enhanced DA, because it provided the best storage performance in the lab-scale experiments, which is discussed later in the results section. This further enabled direct scaling up of the experimental results for capacity and power to suit the conceptual scenarios. The calculations focused on estimating the heating for the coldest winter months (December–February) in Helsinki area when the demand is the highest.

The calculations were made without considering the addition of a heat pump to the system or possible heat losses in the system that could be avoided via a proper insulation. The calculations were made using the design parameters in Table A in the Supplementary Information for a shielded or open space condition for the bus stop. The lower convective heat transfer coefficient for air was applied for the shielded space, while, the higher value was used for the open space exposed to wind. The Fourier's law equation was used to describe the heat flux by means of conduction through the surface of floor or bench:

$$q_x = -k \frac{dT}{dx} \quad (3)$$

where k is the conductivity of the surface material. Newton's law of cooling was used to describe the heat transfer from the floor or bench surface to the surrounding air:

$$Q = hA(T_s - T_a) \quad (4)$$

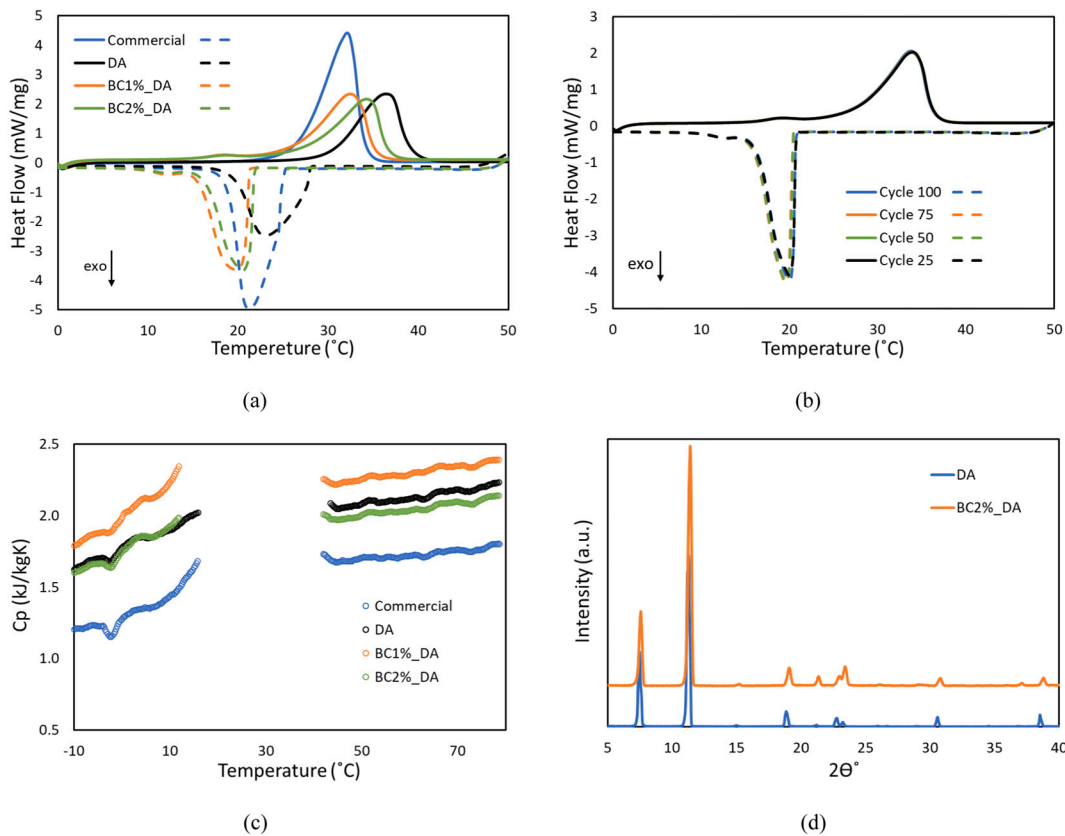


Fig. 3. (a) The DSC heating-cooling curves of pristine and BC-enhanced PCMs and (b) 100 DSC cycling on 2 % BC-enhanced DA under 5 K/min scan rate; (c) C_p graphs of all PCMs within -10 °C to 80 °C temperature range. The phase change interval has been removed for simplicity (Fig. D in Supplementary Information includes the complete temperature range); and (d) XRD patterns of DA and 2 % BC-enhanced DA.

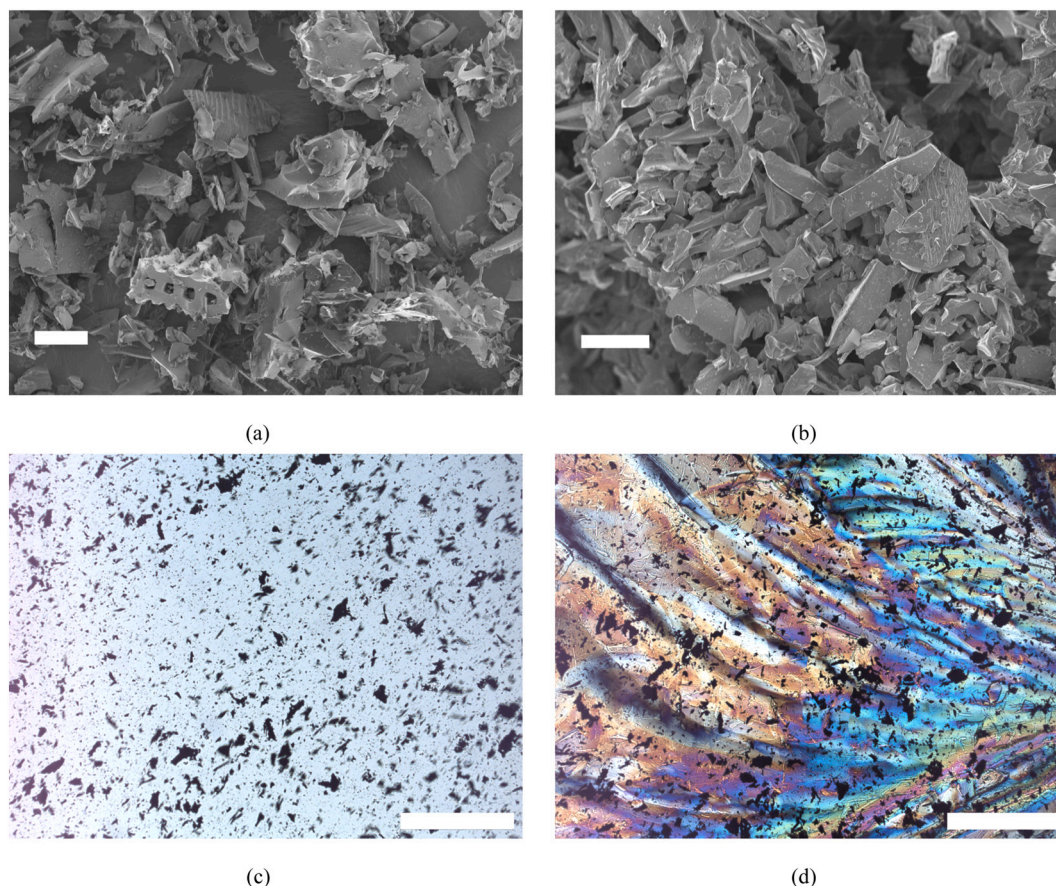


Fig. 4. SEM images of (a) BC and (b) 2 % BC-enhanced DA: the scale bar is 20 μm , and POM images of 2 % BC-enhanced DA samples in (c) liquid and (d) solid phases: the scale bar is 500 μm .

where h and A are the heat transfer coefficient and surface area and T_s and T_a are the temperatures of the surface and the air, respectively. The heat demand in order to keep the floor or the bench surface at 20 °C is therefore:

$$Q_{\text{demand}} = Q_{\text{cond}} = Q_{\text{conv}} \quad (5)$$

The heat flux through the floor equals the convective heat flux away from the floor ($Q_{\text{cond}} = Q_{\text{conv}}$). The required temperature below the floor was derived and calculated with the following formula:

$$T = \frac{hx(T_s - T_a)}{k} + T_s \quad (6)$$

where x is the thickness of floor. Table B in the Supplementary Information provides the required heating demand and price for the floor and the bench of the proposed bus stop with a shielded or open space in -1.17 °C outside temperature.

3. Results and discussion

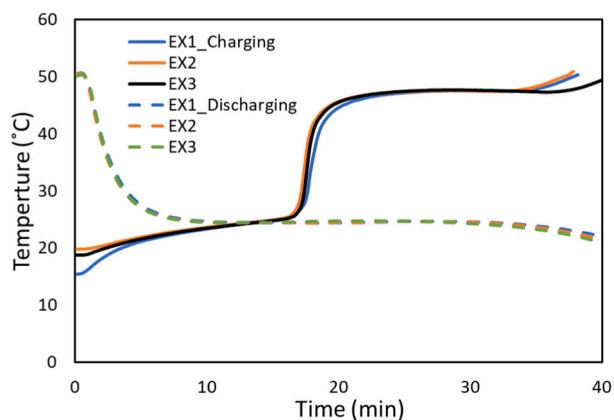
3.1. Characteristics of phase change materials

Table 1 summarizes the thermophysical properties of the PCMs. Fig. 3 shows the DSC curves of the pristine and BC-enhanced PCMs. The PCMs showed melting within 30–36 °C temperature range, which is suitable for low-grade heat storage applications. The enthalpy of phase change ranged between 156 and 248 J/g. Two weight percentages of BC (1 % and 2 %) were examined to further enhance the thermal properties of DA because of its consistent phase change behavior during DSC measurements (see Fig. C in the Supplementary Information). The

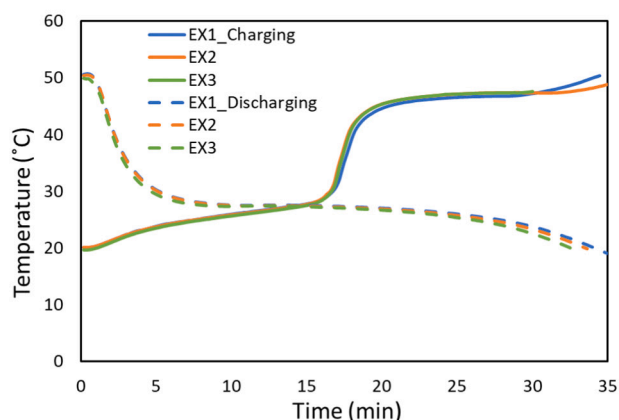
melting and crystallization temperatures of the PCM were lowered after the BC addition, which is consistent with previously reported studies on PCMs with additives [30,31]. This phenomenon can originate from the intermolecular interactions between the additive and the PCM. As can be seen in Figs. 3, 1 % BC shifted the melting peak more than that of 2 % concentration. Interestingly, 1 % BC also increased the latent heat value by 5.8 % (170.5 J/g), whereas 2 % concentration slightly reduced the value by 3.4 % (155.6 J/g).

Fig. 3c include C_p values and plots for solid and liquid states. Fig. D in the supplementary Information shows the complete temperature range. The specific heat increases as the temperature rises, particularly for solid state. The specific heat of liquid phase was higher than that of the solid phase. Similar C_p ranges have been reported for other fatty acid PCMs in the literature [32,33]. Although PCA28 showed a higher latent heat of melting, it had lower specific heat capacities than those of DA. The specific heat of solid state for 1 % BC-enhanced DA was 14 % higher than that of pure DA. For the 2 % BC-enhanced DA, the C_p remained of similar value as that of the pure DA. After melting, the specific heat of 2 % concentration was slightly lower, while 1 % concentration indicated a slightly higher specific heat than that of DA. These results suggest that 1 % concentration of BC performs more effectively in the enhancement of related thermal properties. The C_p of BC ranged within 0.88–1.20 kJ/kgK over 20 °C to 70 °C temperature range. A cycling experiment was performed on BC-enhanced DA to investigate the consistency of its phase change behavior under 100 consecutive melting-crystallization cycles. It can be seen in Fig. 3b that the phase change behavior is repetitive and the PCM's thermal properties are not weakened by cycling.

Fig. 3d shows the XRD patterns of DA and BC-enhanced DA. Both compositions show similar patterns with two characteristic peaks at $2\theta = 7.5^\circ$ and 11.5° , which confirms that the crystal structure of DA remains



(a)

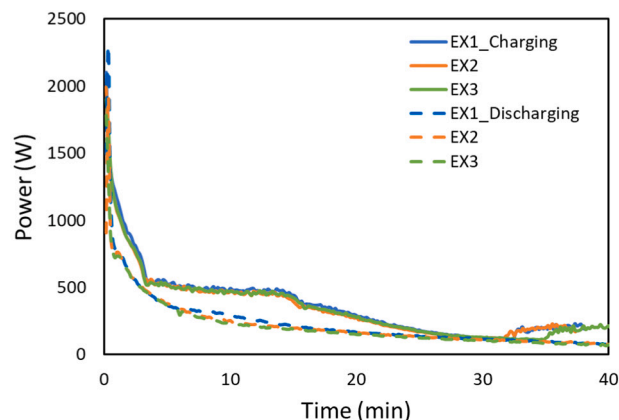


(b)

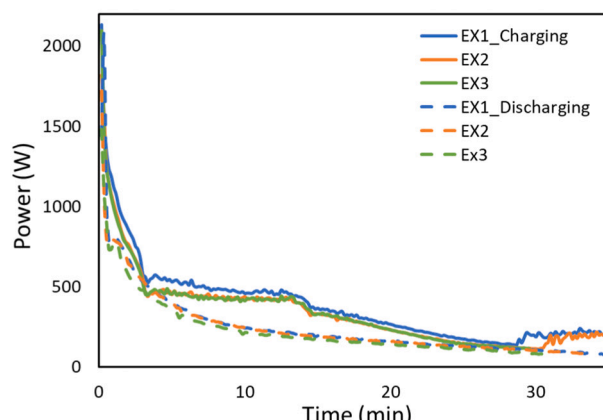
Fig. 5. Temperature levels during charging-discharging cycles for a) PCA28 and b) DA. The temperature is related to thermocouple TC3 shown in Fig. 2. Each plot includes three experiment repetitions (EX1-3) for charging and discharging.

intact after BC addition. Fig. 4 reveals the structural and crystalline morphology of BC and BC-enhanced DA. The BC particles (the dark spots) spread uniformly in both the melt (Fig. 4c) and crystalline (Fig. 4d) states. A movement of particles within the liquid state was observed under the POM, which shows the physical nature of BC and PCM interface. The bright colourful regions in Fig. 4d are ascribed to the crystal phase. The SEM revealed a smooth coverage morphology for the crystalline particles of 2 % BC-enhanced PCM and a porous structure for the BC particles.

As reported in Table 1, the TC values for DA was 0.52, which was increased to 0.6 and 0.62 W/mK by 1 % and 2 % BC concentrations. The TC of pure BC powder was 0.06 W/mK. Note that the biochar sample was measured in a fine powder (particle size smaller than 50 μm), as the form that was applied. Such a low-density powder sample is considered a discontinuous highly porous medium with numerous air-filled voids. The thermal conductivity of these structures measured at room temperature is likely to be influenced by phonon-boundary scattering resulted from the large number of particle boundary contacts and/or junctions. A similar behavior was reported for the thermal conductivity of bulk graphite powder [34]. However, when the biochar particles are added to the PCM, it becomes a continuous solid medium with no to limited pores or voids [29]. All the PCMs samples including biochar enhanced PCMs were measured as a disk-like solid pallet. A picture of biochar powder and PCM disks used in thermal conductivity measurements is provided in the Supplementary Information as Fig. E. A similar enhancement of conductivity was reported for graphite based



(a)



(b)

Fig. 6. Generated power during charging-discharging cycles for a) PCA28 and b) DA versus time of the experiments. Each plot includes three experiment repetitions (EX1-3) for charging and discharging.

composites within this range of additive percentage [35].

3.2. Storage performance of lightweight heat exchanger

The total amount of energy stored by the PCM was calculated with Eq. (1). The storage capacity (Q_s) was 473 kJ for PCA28 and 409 kJ for DA. Fig. 5 illustrates charging and discharging temperature curves for both PCMs. Clear temperature stabilization by the phase change phenomenon is observed for both PCMs during charging and discharging. The duration for melting interval was 14.5 min and 13.8 min, while the complete charging duration ($22^\circ\text{C} \rightarrow 50^\circ\text{C}$) was 26 min and 25 min for PCA28 and DA, respectively. The crystallization interval was 20 min and 19.7 min, while the complete discharging duration ($50^\circ\text{C} \rightarrow 22^\circ\text{C}$) was 42.5 min and 34 min for PCA28 and DA, respectively. The extra long discharging process for PCA28 may originate from its irregular crystallization behavior observed in the DSC results (Fig. C in the Supplementary Information). The grid structure significantly improved the storage performance of the base plate HE [22] from a charging rate of above 200 min (Table 3) to less than 25 min.

Fig. 6 includes the plots of the charging and discharging power. The average power during melting interval, was 494 W and 442 W, while the average power for the complete charging process was 458 W and 429 W for PCA28 and DA, respectively. The average power during crystallization interval was 205 W and 200 W for PCA28 and DA, respectively. Power during the complete discharging process was 212 W for PCA28 and 243 W for DA. The discharging time is longer than the charging time for both PCMs, while the discharging power was also lower than

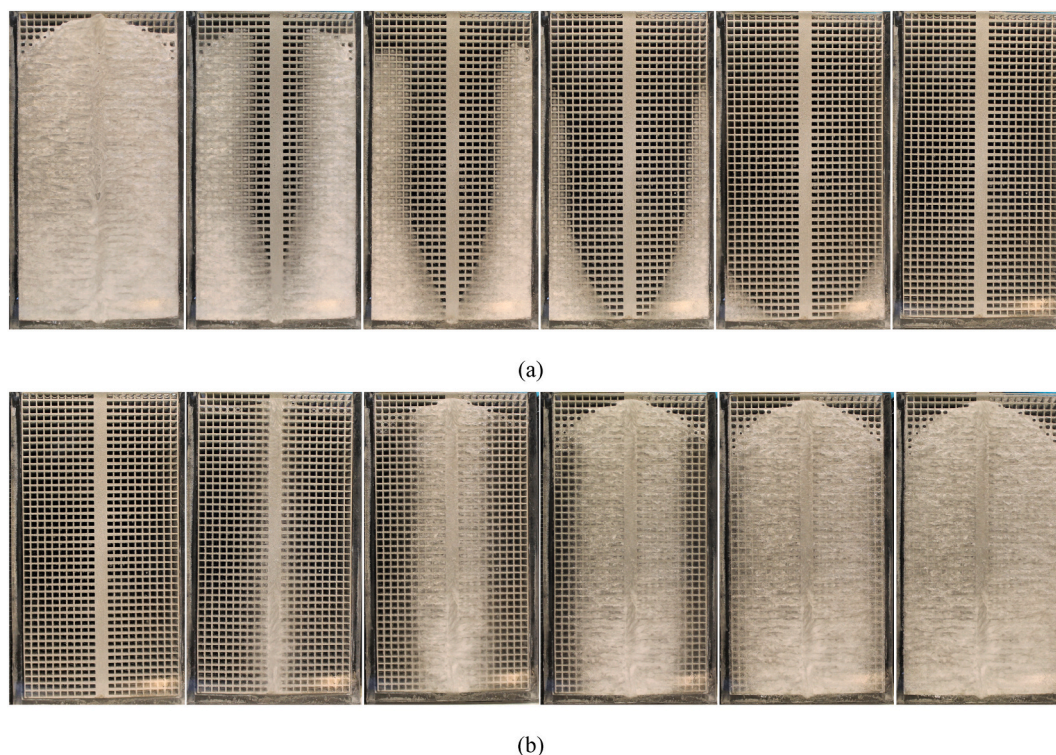


Fig. 7. a) Melting and b) crystallization of pristine DA recorded upon 4 min time intervals. See Fig. G in the Supplementary Information for the pictures of PCA28.

charging power. A reverse behavior was previously observed for grid heat exchangers with higher metal content [22], possibly originating from their higher heat transfer rate, larger operation temperature range, as well as larger difference between the HTF temperature and the melting temperature. The Supplementary Information includes inflow and outflow temperature plots of HTF (Fig. F) for the charging and discharging experiments.

Melting and crystallization of the PCMs were photographed to better visualize the phase change process. Fig. 7 shows the melting of DA at 4 min time intervals between each image. The melting started in the middle part of the LHE, adjacent to the base plate for the HTF circulation. At the beginning, the heat transfer was driven by conduction from LHE to the solid PCM. When the PCM began to melt, the heat transfer shifted to both conduction and some level of natural convection by the melt, which is consistent with previous observations [19,22].

The PCM in the top part of the tank melted faster compared with that of the lower part due to the natural convection assisted motion of the melt. The density gradient between the melt and solid states causes buoyancy driven convection and forces the melt to ascend upward in the tank. This can lead to a temperature stratification in the tank, where the upper region is dominated by SHS and lower part of the tank is dominated by LHS. Thus, the solid at the bottom melts with a slower rate. The effect of natural convection was less dominant in the grid HEs with a higher metal content reported in our previous work [22], which can be due to their greater conductive heat transfer rate.

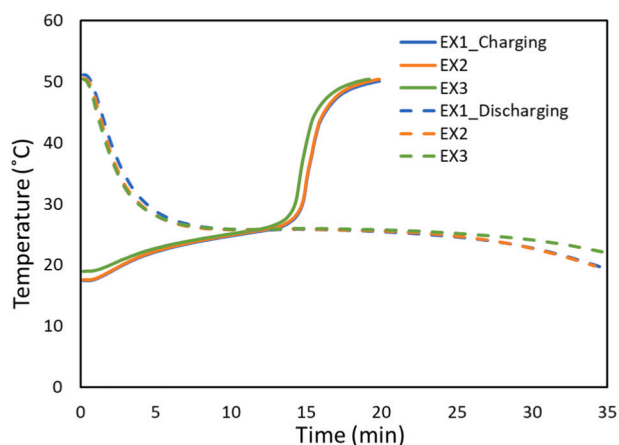
Fig. 7 pictures the crystallization of DA upon 4 min time intervals. Crystallization started at the base plate and progressed evenly toward the edges of the tank. Immediately after the crystallization initiation, a solid layer covered the surface of the base plate. This hinders the natural convection motion of the liquid [22] and allows the PCM to solidify more evenly throughout the tank. Between the two PCMs (Fig. 7 and Fig. G in the Supplementary Information), DA crystallized more evenly in the horizontal direction. This indicates that the discharging rate is more effective within DA-based storage, which is also confirmed by the discharging data and DSC measurements. Complete discharging duration was 25 % faster and the discharging power for the entire cycle was

15 % higher for DA than those of PCA28.

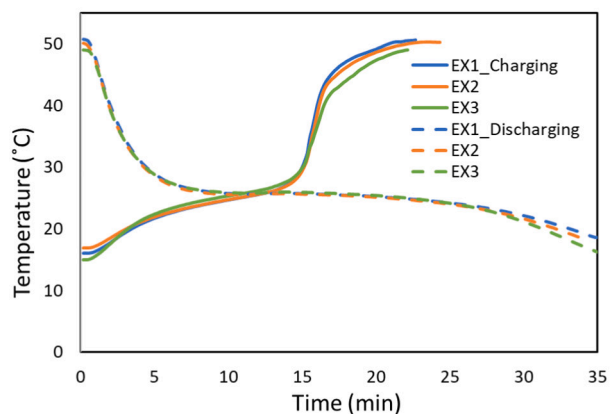
Previously, melting and crystallization of PCM in a double tube fin-based HE was numerically examined to understand the effect of the fin characteristics on the storage performance [36]. The use of straight fins reduced the process time more effectively than that of locally arranged fins, e.g. lower fins or upper fins. Interestingly, lower arrangement of the fins could accelerate melting but significantly delayed crystallization. Longer fins enhanced the heat transfer more efficiently than shorter fins. The melting process of PCMs inside a triplex HE with double-sided heat transfer was numerically studied using three layers PCMs with different melting temperatures in combination with Al6061 metal foam [37]. Using three layers of PCMs hindered the melting rate by 35 %, but the metal foam greatly increased the melting rate with enhancing the thermal conductivity and created a more uniform distributed temperature. Metal foams were also used for the thermal conductivity enhancement of a refrigeration battery for cold chain transport [38].

3.3. Simultaneous effect of biochar additive

Although the lightweight heat exchanger was powerful and fast to charge (409 kJ storage capacity and 442 W charging power over 13.8 min of melting duration), the addition of BC additives was investigated to further enhance the system performance. The total amount of energy (Q_c) stored in BC enhanced DA was 444 kJ with 1 % BC and 408 kJ with 2 % BC. The configuration with 1 % BC concentration provided a higher heat storage capacity (19 % increase) than pure DA thanks to the increase in its specific and latent heat values. The charging temperatures of DA with both BC concentrations can be seen in Fig. 8. Melting duration was 11.9 min for 1 % and 12.3 min for 2 % concentrations. When compared with that of pure DA (13.8 min), the melting time was reduced by 14 %. The complete charging duration was significantly faster for both BC concentrations (by 33 % reduction). The configuration with 1 % BC took 16.8 min and the one with 2 % BC required 18.7 min to charge completely, whereas pure DA took 25 min. This indicates that the thermal performance improves with the addition of BC particles and a



(a)



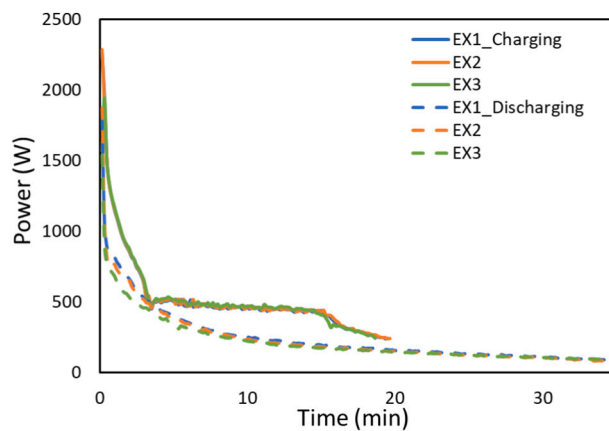
(b)

Fig. 8. Temperature levels during charging-discharging cycles for a) 1 % BC-enhanced DA and b) 2 % BC-enhanced DA. The temperature is related to thermocouple TC3 shown in Fig. 2. Each plot includes three experiment repetitions (EX1-3) for charging and discharging.

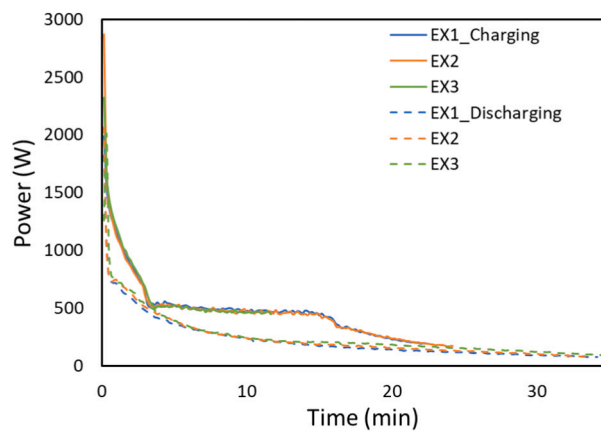
lower BC concentration results in a more desired outcome, which is consistent with the DSC results. Supplementary Information (Section 5) includes further details of comparing LHE with the heavier designs from our previous work [22].

Fig. 9 illustrates the charging power for DA with both of added BC concentrations. The average charging power during melting interval was 501 W for 1 % concentration and 512 W for 2 % concentration. When compared with that of pure DA, the melting power increased 13 % and 16 % for 1 % and 2 % concentrations, respectively. Regarding the complete charging process, the increase in power by the additive is more significant, as 1 % resulted in 32 % and 2 % resulted in 28 % power increase. This indicates that BC addition also improves SHS by the system, confirming the C_p results. The crystallization duration was 19.2 min for 1 % BC, 0.5 min faster than that of pure DA, and 19.8 min for 2 % BC. As DSC results indicated, the crystallization process behaves more irregularly than the melting process, which is also evident when looking at the complete discharging duration. Fig. 9 illustrates discharging power of both BC concentrations. Average discharging power was 191 W and 194 W for 1 % and 2 % BC concentrations, respectively. The system results are in alignment with the DSC results for both BC concentrations: 1 % concentration resulted in larger improvements in charging time and power than those of 2 % concentration. Table 2 provides a summary of the experimental results with DA and BC-enhanced DA.

The distribution of a PCM in a multi-tube HE was numerically investigated to reduce the crystallization time [39]. Different fractions



(a)



(b)

Fig. 9. Generated power during charging-discharging cycles for a) 1 % BC-enhanced DA and b) 2 % BC-enhanced DA versus time of the experiments. Each plot includes three experiment repetitions (EX1-3) for charging and discharging.

Table 2

Storage performance of the LHS system with different PCMs and BC additives.

Type of PCM	PCA28	DA	1 % BC	2 % BC
Melting power (W)	494	442	501	512
Overall charging power (W)	458	429	568	550
Melting duration (min)	14.5	13.8	11.9	12.3
Overall charging duration (min)	25.9	25	16.8	18.7
Crystallization power (W)	205	200	191	194
Overall discharging power (W)	212	243	232	234
Crystallization duration (min)	20	19.7	19.2	19.8
Overall discharging duration (min)	42.5	34	35	33.3
Storage capacity (kJ)	473	409	444	408
Mass of PCM (g)	1584	1844	1863	1881

of copper nano-particles were mixed with the PCM filled in the inner and outer tubes of the HE, while the HTF flowed in between these two tubes. A proper PCM mass distribution resulted in 62 % decrease in the crystallization duration, while increasing the nano-particles volume fractions to 4 % reduced the time by 15 %. Table 3 presents the storage performance of different HEs that have been experimentally studied for LHS utilizing different PCMs. Experimental parameters such as the mass flow rate of the HTF, the size of the storage, as well as the type and amount of loaded PCM are among influential factors on the storage characteristics.

Fig. 10 visually depicts the charging and discharging processes of DA

Table 3

The storage performance of different heat exchangers with PCMs reported in the literature and this work. The maximum power and time are related to charging process.

HE	Max Power W	Time min	PCM	Melting °C	PCM Mass kg
Copper fin [18]	1220	67	Paraffin	55–60	3.2
Pillow plate [40]	2700	83	SAT	59	30
Shell-tube [41]	300	150	paraffin	44–54	4
Plate [22]	140	250	paraffin	56	1.80
Grid [22]	2500	20	paraffin	56	1.59
Biochar-grid	3000	19	DA	36	1.88

with 2 % BC additive. The pictures are recorded at 4 min time intervals and the duration from the first to the last picture is 20 min. It can be seen that upon 4–8 min of melting, the liquid ascended to the upper part of the container due to its lower density. The addition of 2 % BC reduced the charging duration by 1.5 min. The melting process of pure DA (Fig. 7a) indicated an vertically inclined shape, suggesting the presence of vertical motion for the PCM melt and some level of temperature stratification in the storage tank. With BC additive, this phenomenon is alleviated, and the PCM melts more evenly with an almost vertically straight shape propagation from the base plate to the edges of the tank. This suggests a less influence of natural convection and instead, the heat transfer is more effective through a combined effect of the grid and additive-assisted conduction.

The shape of crystallization also altered from that of pure DA in

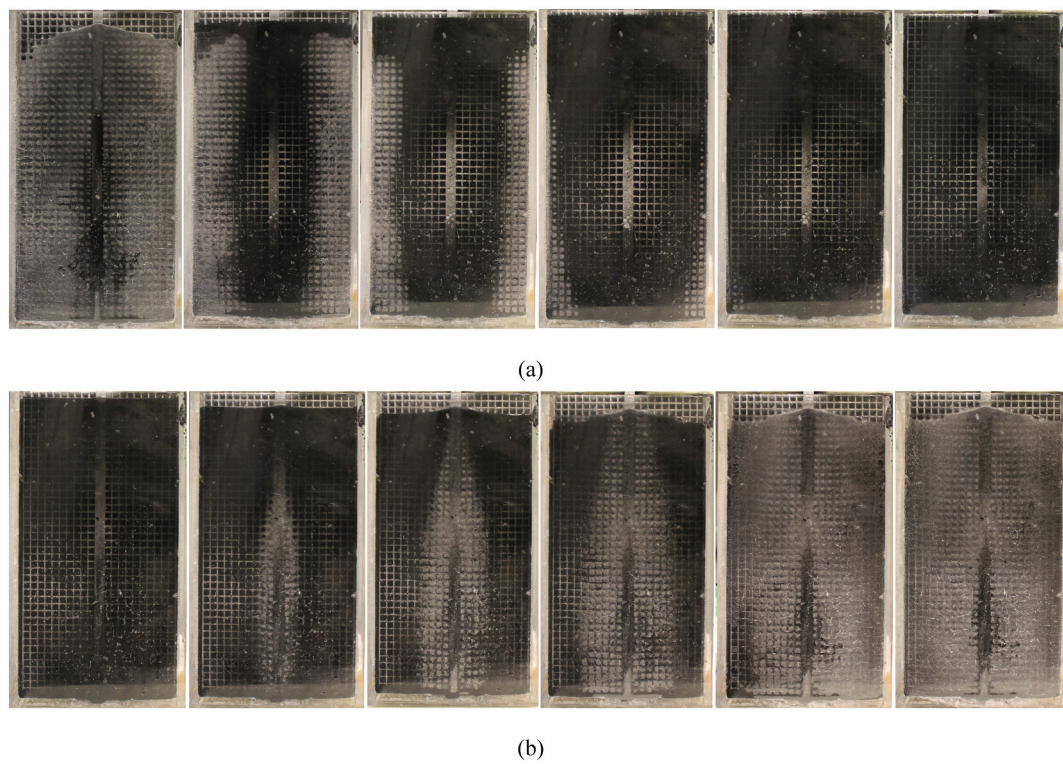


Fig. 10. a) Melting and b) crystallization of DA with 2 % BC additive documented at 4 min time intervals.



Fig. 11. The LHS heating concept for the bench and floor of a smart city bus stop: a) the open view of the bench and b) the floor heating storage located inside or underground. See Fig. H of the Supplementary Information for more illustrations. Images were made by Design Factory Team in Aalto University.

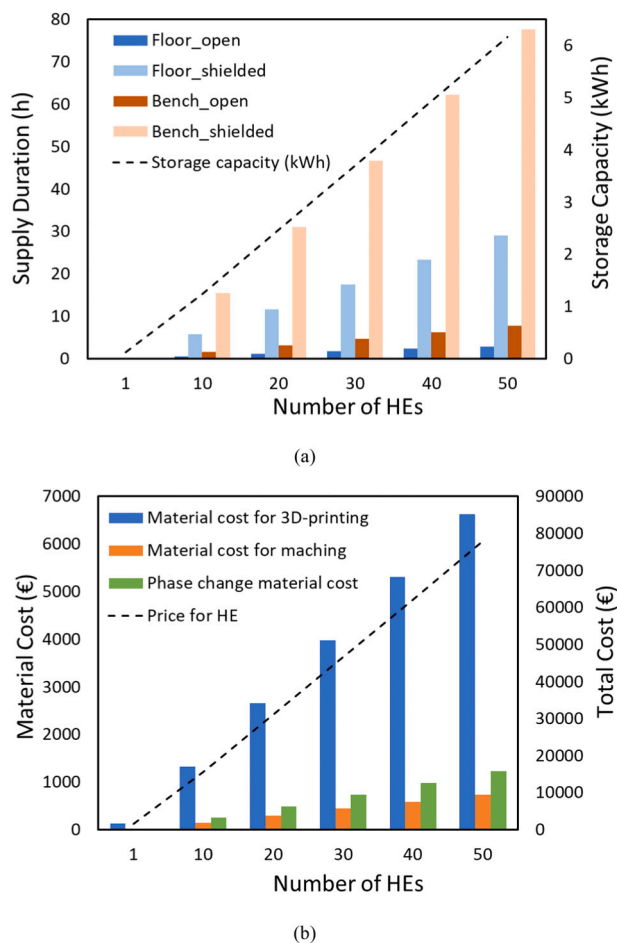


Fig. 12. a) Supply duration and storage capacity versus the number of integrated LHE in a conceptual design of a smart city bus stop and b) material and total costs for the PCM and LHE production.

Fig. 7. Pure DA crystallized with a vertically straight shape, but after BC addition it crystallized unevenly in the vertical direction with a slightly slower rate at the upper region of the tank. The BC particles may settle during crystallization due to the lack of natural convection, leading to higher crystallization rate at the bottom of the tank. Most likely, this is the reason for a longer charging process of DA with BC additives than that of pure DA. This can be prevented by lowering the BC concentration to 1 %.

3.4. Conceptual application scenarios

To further portrait the potential integration of such LHS into real-world scenarios, a conceptual design was developed based upon the lab-scale experimental results. The proposed conceptual design featured modular LHS components packed together to enable scaling-up the system in a variety of sizes. Fig. 11 illustrates the conceptual design to heat up a bus stop bench with a smaller modular LHS unit integrated inside the bench and a bus stop floor with a larger unit located underground (see Fig. H in the Supplementary Information for more illustrations). The modularity is achieved by coupling of LHE series in a large PCM container. Aside from a modular solution, the grid design of an individual LHE could also be enlarged from the base plate to the sides to reduce the number of separate HEs integrated in the system.

Such a system can be connected to a low temperature district heating (LTDH) network, for example the LTDH under construction in the Kera area of Finland. The LTDH network can facilitate the integration of LHS unit through its existing infrastructure, location accessibility, and

continuous heat supply (50 °C). Furthermore, LTDH is increasingly utilizing various waste heat streams from industries, data centers, pharmaceutical centers as well as 5G network [42]. The supply of energy from stand-alone sources e.g. 5G radio towers or data centers, however, might restrict the location of the storage and continuity of the energy input. The integration of LHS can simultaneously balance load fluctuations in LTDH and stabilize return water temperatures to its substations [43]. The fluctuation in heating demand between end-users is a major challenge for the efficiency of LTDH, causing an undesired increase in the return water temperature to the substations [43,44]. The return water is usually cooled by disposing the excess heat to the environment using cooling towers, which is unsustainable and wastes heat. Centralized SHS tank have been unsuccessful in storing this excess heat from the substation return water. LHS units installed at the substation return water pipe, however, has been reported to lower the return water temperature through simultaneous storage of 70 % surplus heat and an increase of the system efficiency (by 22 %) [43]. In the context of our conceptual scenarios, the excess heat from LTDH substation return water could possibly be used to charge the bus stop storage, given that it is located near the substation.

Fig. 12 indicates the heating duration for the floor and the bench in the shielded space depending on the size of the storage. For instance, a 42-l LHS is required for 12 h heating of the floor area in a shielded space with 2.5 kWh capacity. This is a valuable asset for load shifting during fluctuations of energy supply or price. The storage can last ten times longer and demands ten times less energy for a shielded space than for an open space. See Table B in the Supplementary Information for the estimated heating demand and prices. The heating supply for a bench lasts 63 % longer than heating supply for a floor, which is directly proportional to the heated area. Therefore, a shielded space allows using a smaller storage configuration to reach significant performance and reduces the expenses.

A bottleneck for this conceptual design, however, is the 3D-printing production cost. The price of the proposed storage includes the cost of PCM and the total material and production costs of the HE series. The high price mainly originates from the fairly new and expensive metal-based 3D-printing production method for the HEs. The cost of AlSi10Mg metal powder (75–145 €/kg) used in the 3D-printing that ranges approximately between 4 and 9 % of the total production cost. Other less expensive manufacturing techniques could therefore be considered in order to lower the production cost. For instance, machining is a cheaper production method and the cost per manufactured can be reduced as the size of production increases. The costs for the raw materials used in machining, i.e. aluminum (2.2 €/kg), is also only 1.5–3 % of the price for AlSi10Mg powder used in 3D-printing. Thus, switching the manufacturing technique to machining can significantly lower the total cost. However, this may impact the characteristics of the HE due to inability to produce highly complex grid structure or the changing of the raw material from AlSi10Mg to aluminum.

4. Conclusions

This investigation aimed at improving the storage performance of a LHS through the positive effect of BC additives on the PCM embedded in a lightweight grid HE. The HE was 3D-printed to provide highly complex extended metal surfaces to enhance the heat transfer, yet to be light in mass with sufficient free space for a large loading of PCM. To further improve the thermal performance of the storage, the PCM was also combined with 1 % or 2 % concentration (wt %) of BC additive. The characterization measurements revealed that the melting and crystallization temperatures were slightly lowered after introducing BC additive to the pristine PCM. Addition of 1 % BC improved the latent heat of melting by 6 %, the latent heat of crystallization by 13.8 % and specific heat of the solid state by 14 %. System level experiments indicated that both concentrations of the additive significantly improve the charging rate of the storage system, which increased up to 32 % (568 W) and 28 %

(550 W) for 1 % and 2 % concentrations, respectively, compared with that of pristine PCM (429 W). Charging duration was notably reduced by 33 % to 16.5 min for 1 % concentration compared with that of pristine PCM (25 min). The system level results were in alignment with the material characterization, with 1 % BC concentration resulting in the most effective improvement in charging energy, power, and time than those of 2 % concentration or pristine PCM. This may be caused by possible agglomeration or settlement of particles in higher concentration within the storage tank. A conceptual modular design of ten integrated LHE and BC enhanced PCM could provide 1.2 kWh heat storage capacity to heat up the floor of a smart city bus stop for 6 h and its bench for 12 h. Such a conceptual design could be connected to the low temperature district heating to supply its energy demand and simultaneously act as a buffer for its temperature fluctuations.

CRedit authorship contribution statement

Maryam Roza Yazdani: Conceptualization, Investigation, Methodology, Formal analysis, Visualization, Supervision, Resources, Writing – original draft, Funding acquisition. **Anna Lagerström:** Conceptualization, Investigation, Methodology, Formal analysis, Visualization. **Ville Vuorinen:** Conceptualization, Supervision, Resources, Writing – review & editing, Funding acquisition.

Declaration of competing interest

The authors declare that there is no conflict of interest.

Data availability

Data will be made available on request.

Acknowledgement

This work was financially supported by the Academy of Finland (343192) and Business Finland (Dnro 1558/31/2019). The authors thank Kari Saari for the assistance with the system set-up and Kirsi Kukko for the 3D-printing design of the heat exchanger. The conceptualization visualization was made by the Design Factory Team in Aalto University.

Appendix A. Supplementary data

Supplementary data to this article can be found online at <https://doi.org/10.1016/j.est.2022.105478>.

References

- [1] L.F. Cabeza, A. de Gracia, G. Zsembinszki, E. Borri, Perspectives on thermal energy storage research, *Energy* 231 (2021), 120943.
- [2] S. Tetteh, M.R. Yazdani, A. Santasalo-Aarnio, Cost-effective electro-thermal energy storage to balance small scale renewable energy systems, *J. Energy Storage* 41 (2021), 102829.
- [3] K. Turunen, M.R. Yazdani, S. Puupponen, A. Santasalo-Aarnio, A. Seppälä, Cold-crystallizing erythritol-polyelectrolyte: scaling up reliable long-term heat storage material, *Appl. Energy* 266 (2020), 114890.
- [4] S.N. Gunasekara, R. Pan, J.N. Chiu, V. Martin, Polyols as phase change materials for surplus thermal energy storage, *Appl. Energy* 162 (2016) 1439–1452.
- [5] J.P. Da Cunha, P. Eames, Thermal energy storage for low and medium temperature applications using phase change materials—a review, *Appl. Energy* 177 (2016) 227–238.
- [6] H. Badenhorst, A review of the application of carbon materials in solar thermal energy storage, *Sol. Energy* 192 (2019) 35–68.
- [7] A.S. Fleischer, *Thermal Energy Storage Using Phase Change Materials: Fundamentals and Applications*, Springer, 2015.
- [8] S. Morales-Ruiz, J. Rigola, C. Oliet, A. Oliva, Analysis and design of a drain water heat recovery storage unit based on pcm plates, *Appl. Energy* 179 (2016) 1006–1019.
- [9] A. Thomson, G. Claudio, The technical and economic feasibility of utilising phase change materials for thermal storage in district heating networks, *Energy Procedia* 159 (2019) 442–447.
- [10] X. Sun, Q. Zhang, M.A. Medina, Y. Liu, S. Liao, A study on the use of phase change materials (pcms) in combination with a natural cold source for space cooling in telecommunications base stations (tbss) in China, *Appl. Energy* 117 (2014) 95–103.
- [11] X. Xiao, P. Zhang, M. Li, Thermal characterization of nitrates and nitrates/expanded graphite mixture phase change materials for solar energy storage, *Energy Convers. Manag.* 73 (2013) 86–94.
- [12] W. Wu, G. Zhang, X. Ke, X. Yang, Z. Wang, C. Liu, Preparation and thermal conductivity enhancement of composite phase change materials for electronic thermal management, *Energy Convers. Manag.* 101 (2015) 278–284.
- [13] R. Baby, C. Balaji, Experimental investigations on phase change material based finned heat sinks for electronic equipment cooling, *Int. J. Heat Mass Transf.* 55 (5–6) (2012) 1642–1649.
- [14] P. Bose, V.A. Amirtham, A review on thermal conductivity enhancement of paraffinwax as latent heat energy storage material, *Renew. Sust. Energy Rev.* 65 (2016) 81–100.
- [15] L. Kalapala, J.K. Devanuri, Influence of operational and design parameters on the performance of a pcm based heat exchanger for thermal energy storage—a review, *J. Energy Storage* 20 (2018) 497–519.
- [16] J. Wei, Y. Kawaguchi, S. Hirano, H. Takeuchi, Study on a pcm heat storage system for rapid heat supply, *Appl. Therm. Eng.* 25 (17–18) (2005) 2903–2920.
- [17] A. Trp, An experimental and numerical investigation of heat transfer during technical grade paraffin melting and solidification in a shell-and-tube latent thermal energy storage unit, *Sol. Energy* 79 (6) (2005) 648–660.
- [18] K. Merlin, D. Delaunay, J. Soto, L. Traonvouez, Heat transfer enhancement in latent heat thermal storage systems: comparative study of different solutions and thermal contact investigation between the exchanger and the pcm, *Appl. Energy* 166 (2016) 107–116.
- [19] M. Avci, M.Y. Yazici, Experimental study of thermal energy storage characteristics of a paraffin in a horizontal tube-in-shell storage unit, *Energy Convers. Manag.* 73 (2013) 271–277.
- [20] K. El Omari, T. Kousksou, Y. Le Guer, Impact of shape of container on natural convection and melting inside enclosures used for passive cooling of electronic devices, *Appl. Therm. Eng.* 31 (14–15) (2011) 3022–3035.
- [21] J. Fukai, M. Kanou, Y. Kodama, O. Miyatake, Thermal conductivity enhancement of energy storage media using carbon fibers, *Energy Convers. Manag.* 41 (14) (2000) 1543–1556.
- [22] M.R. Yazdani, A. Laitinen, V. Helaakoski, L.K. Farnas, K. Kukko, K. Saari, V. Vuorinen, Efficient storage and recovery of waste heat by phase change material embedded within additively manufactured grid heat exchangers, *Int. J. Heat Mass Transf.* 181 (2021), 121846.
- [23] K. Yuan, J. Shi, W. Aftab, M. Qin, A. Usman, F. Zhou, Y. Lv, S. Gao, R. Zou, Engineering the thermal conductivity of functional phase-change materials for heat energy conversion, storage, and utilization, *Adv. Funct. Mater.* 30 (8) (2020) 1904228.
- [24] D.G. Atinafu, B.Y. Yun, S. Wi, Y. Kang, S. Kim, A comparative analysis of biochar, activated carbon, expanded graphite, and multi-walled carbon nanotubes with respect to pcm loading and energy-storage capacities, *Environ. Res.* 195 (2021), 110853.
- [25] O. Tomin, R. Vahala, M.R. Yazdani, Tailoring metal-impregnated biochars for selective removal of natural organic matter and dissolved phosphorus from the aqueous phase, *Microporous Mesoporous Mater.* 328 (2021), 111499.
- [26] G. Hekimoğlu, A. Sari, S. Arunachalam, H. Arslanoğlu, O. Gencel, Porous biochar/heptadecane composite phase change material with leak-proof, high thermal energy storage capacity and enhanced thermal conductivity, *Powder Technol.* 394 (2021) 1017–1025.
- [27] L. Desgrosseilliers, C.A. Whitman, D. Groulx, M.A. White, Dodecanoic acid as a promising phase-change material for thermal energy storage, *Appl. Therm. Eng.* 53 (1) (2013) 37–41.
- [28] Y. Li, H. Yan, Q. Wang, H. Wang, Y. Huang, Structure and thermal properties of decanoic acid/expanded graphite composite phase change materials, *J. Therm. Anal. Calorim.* 128 (3) (2017) 1313–1326.
- [29] A. Seppälä, K. Turunen, M.R. Yazdani, Thermal conductivity of sugar alcohols, *Sol. Energy Mater. Sol. Cells* 243 (2022), 111796.
- [30] M.R. Yazdani, J. Etula, J.B. Zimmerman, A. Seppälä, Ionic cross-linked polyvinyl alcohol tunes vitrification and cold-crystallization of sugar alcohol for long-term thermal energy storage, *Green Chem.* 22 (16) (2020) 5447–5462.
- [31] M.R. Yazdani, R. Ajdary, A. Kankkunen, O.J. Rojas, A. Seppala, Cellulose nanofibrils endow phase-change polyethylene glycol with form control and solid-to-gel transition for thermal energy storage, *ACS Appl. Mater. Interfaces* 13 (5) (2021) 6188–6200.
- [32] L. Shilei, Z. Neng, F. Guohui, Eutectic mixtures of capric acid and lauric acid applied in building wallboards for heat energy storage, *Energy Build.* 38 (6) (2006) 708–711.
- [33] C. Yadav, R.R. Sahoo, Experimental analysis for optimum thermal performance and thermophysical parameters of mwcnt based capric acid pcm by using t-history method, *Powder Technol.* 364 (2020) 392–403.
- [34] N. Pradhan, H. Duan, J. Liang, G. Iannacchione, The specific heat and effective thermal conductivity of composites containing single-wall and multi-wall carbon nanotubes, *Nanotechnology* 20 (24) (2009), 245705.
- [35] T. C. Mokhena M. J. Mochane J. S. Sefadi S. V. Motloung D. M. Andala n.d. Thermal conductivity of graphite-based polymer composites, *Impact of Thermal Conductivity on Energy Technologies* 181.
- [36] C. Nie, S. Deng, J. Liu, Effects of fins arrangement and parameters on the consecutive melting and solidification of pcm in a latent heat storage unit, *J. Energy Storage* 29 (2020), 101319.

- [37] M.H.S. Abandani, D.D. Ganji, Melting effect in triplex-tube thermal energy storage system using multiple pcms-porous metal foam combination, *J. Energy Storage* 43 (2021), 103154.
- [38] J. Tarragona, W. Beyne, A. de Gracia, L.F. Cabeza, M. De Paepe, Experimental analysis of a latent thermal energy storage system enhanced with metal foam, *J. Energy Storage* 41 (2021), 102860.
- [39] M. Gorzin, M.J. Hosseini, M. Rahimi, R. Bahrampoury, Nanoenhancement of phase change material in a shell and multi-pcm-tube heat exchanger, *J. Energy Storage* 22 (2019) 88–97.
- [40] W. Lin, W. Zhang, Z. Ling, X. Fang, Z. Zhang, Experimental study of the thermal performance of a novel plate type heat exchanger with phase change material, *Appl. Therm. Eng.* 178 (2020), 115630.
- [41] M. Hosseini, M. Rahimi, R. Bahrampoury, Experimental and computational evolution of a shell and tube heat exchanger as a pcm thermal storage system, *Int. Commun. Heat Mass Transfer* 50 (2014) 128–136.
- [42] A. Khosravi, T. Laukkanen, V. Vuorinen, S. Syri, Waste heat recovery from a data Centre and 5g smart poles for low-temperature district heating network, *Energy* 218 (2021), 119468.
- [43] M. Turski, K. Nogaj, R. Sekret, The use of a pcm heat accumulator to improve the efficiency of the district heating substation, *Energy* 187 (2019), 115885.
- [44] D. Schmidt, A. Kallert, M. Blesl, S. Svendsen, H. Li, N. Nord, K. Sipilä, Low temperature district heating for future energy systems, *Energy Procedia* 116 (2017) 26–38.